J Neurophysiol 102: 2358–2374, 2009.
First published August 12, 2009; doi:10.1152/jn.91346.2008.

Coding of Repetitive Transients by Auditory Cortex on Heschl's Gyrus

John F. Brugge,[1,2] Kirill V. Nourski,[1] Hiroyuki Oya,[1] Richard A. Reale,[1,2] Hiroto Kawasaki,[1] Mitchell Steinschneider,[3] and Matthew A. Howard III[1]

[1]*Department of Neurosurgery, University of Iowa, Iowa City, Iowa;* [2]*Departments of Psychology and Physiology, University of Wisconsin, Madison, Wisconsin; and* [3]*Departments of Neurology and Neuroscience, Albert Einstein College of Medicine, New York, New York*

Submitted 19 December 2008; accepted in final form 9 August 2009

Brugge JF, Nourski KV, Oya H, Reale RA, Kawasaki H, Steinschneider M, Howard MA. Coding of repetitive transients by auditory cortex on Heschl's gyrus. *J Neurophysiol* 102: 2358–2374, 2009. First published August 12, 2009; doi:10.1152/jn.91346.2008. The capacity of auditory cortex on Heschl's gyrus (HG) to encode repetitive transients was studied in human patients undergoing surgical evaluation for medically intractable epilepsy. Multicontact depth electrodes were chronically implanted in gray matter of HG. Bilaterally presented stimuli were click trains varying in rate from 4 to 200 Hz. Averaged evoked potentials (AEPs) and event-related band power (ERBP), computed from responses at each of 14 recording sites, identified two auditory fields. A core field, which occupies posteromedial HG, was characterized by a robust polyphasic AEP on which could be superimposed a frequency following response (FFR). The FFR was prominent at click rates below ~50 Hz, decreased rapidly as click rate was increased, but could reliably be detected at click rates as high as 200 Hz. These data are strikingly similar to those obtained by others in the monkey under essentially the same stimulus conditions, indicating that mechanisms underlying temporal processing in the auditory core may be highly conserved across primate species. ERBP, which reflects increases or decreases of both phase-locked and non–phase-locked power within given frequency bands, showed stimulus-related increases in gamma band frequencies as high as 250 Hz. The AEPs recorded in a belt field anterolateral to the core were typically of low amplitude, showing little or no evidence of short-latency waves or an FFR, even at the lowest click rates used. The non–phase-locked component of the response extracted from the ERBP showed a robust, long-latency response occurring here in response to the highest click rates in the series.

INTRODUCTION

Primary auditory cortex in humans occupies the posteromedial portion of the anterior transverse gyrus—hereafter referred to as Heschl's gyrus (HG)—on the superior temporal plane, deep within the lateral fissure. Although this area has the basic cellular structure associated with koniocortex, it is not uniform in its cytoarchitecture and thus appears composed of multiple "primary" and "primary-like" variants (Fullerton and Pandya 2007; Galaburda and Sanides 1980; Hackett et al. 2001; Morosan et al. 2001, 2005). These koniocortical fields of human are considered to be homologous with the tripartite auditory "core" cortex of nonhuman primates (Hackett 2003, 2007; Hackett et al. 2001; Sweet et al. 2005). Core cortical fields in nonhuman primates receive their main thalamic input largely in parallel from the ventral division of the medial geniculate body (de la Mothe et al. 2006; Morel et al. 1993) and, hence, preserve both temporal and spectral information with a high degree of fidelity (Bendor and Wang 2008). Immediately surrounding the auditory core is a belt of cortex made up of multiple fields, which are anatomically and chemically distinct from one another and from the auditory core (Chiry et al. 2003; Fullerton and Pandya 2007; Hackett et al. 1998, 2001; Rivier and Clarke 1997; Wallace et al. 2002). Homologies with the belt fields in the macaque monkey are less certain than those of the auditory core (reviewed by Hackett 2007). Belt fields of the monkey exhibit characteristic architectonic and connectivity patterns that make them functionally distinguishable from each other and from the core by their neuronal response timing, spectral selectivity, tonotopy, binaural sensitivity, and enhanced responsiveness to complex sound, including primate vocalization (Bieser and Müller-Preuss 1996; Kaas and Hackett 2005; Oshurkova et al. 2008; Rauschecker and Tian 2004; Rauschecker et al. 1995; Recanzone et al. 2000; Tian et al. 2001; Woods et al. 2006).

Physiological and anatomical data are consistent with a working model of hierarchical, serial-parallel processing of acoustic information at the cortical level in monkey (Kaas and Hackett 2005; Rauschecker 1998; Rauschecker et al. 1997). The fact that certain features of auditory cortex are shared between humans and nonhuman primates has also made this model an attractive starting point for understanding the functional organization of auditory cortex in human (Hackett 2007; Rauschecker 1998; Wessinger et al. 2001). To determine the extent to which common organizational principles are shared across primate species, including humans, it would be best if the same or similar experimental methods and approaches are used. To this end, we have been recording directly from the auditory cortex of human neurosurgical patients, systematically analyzing response properties over a wide range of acoustic stimuli, including those commonly used in studies of auditory cortex of nonhuman primates.

In this study, we focus attention on temporal processing of repetitive acoustic transients by auditory core and belt fields of HG previously identified on physiological grounds (Brugge et al. 2008b; Liegeois-Chauvel et al. 1991). Considerable information is available on the temporal fidelity of core fields to click-train stimulation in awake New World (Lu et al. 2001) and Old World (Steinschneider et al. 1998) monkeys. By using essentially the same stimuli as used in the monkey experiments, we have been able to compare directly our results obtained from human core cortex with those obtained from homologous cortex in monkeys. Temporal locking to successive transients by neurons or neuronal assemblies in core cortex of a number of mammalian species, including nonhuman primates, has been shown to correlate with human perceptual phenomena, including acoustic flutter, roughness, and

Address for reprint requests and other correspondence: J. F. Brugge, Dept. of Psychology, Brogden Hall, 1210 West Johnson St., Univ. of Wisconsin, Madison, WI 53705 (E-mail: brugge@physiology.wisc.edu).

temporal pitch, and in the speech realm, with voice onset time (Eggermont 1995; Fishman et al. 2000, 2001; Lu et al. 2001; Steinschneider et al. 1993, 1994, 1995a,b 1998, 2005). Similarly, using click-train stimulation has also allowed us to relate directly the fidelity of temporal encoding by human core cortex to these perceptual phenomena (see also Liegeois-Chauvel et al. 1999; Steinschneider et al. 1998).

We reported previously that a robust polyphasic average-evoked potential (AEP), localized to the auditory core in posteromedial HG, is elicited by a brief, 100-Hz click train (Brugge et al. 2008b). This evoked waveform includes a superimposed frequency following response (FFR). The waveform typically recorded on a putative belt field in anterolateral HG is, in contrast, characterized by relatively low-amplitude, long-latency deflections, and the FFR is not in evidence, at least at a click rate of 100 Hz. Studies in experimental animals (Brosch et al. 2002; Steinschneider et al. 2008) and human subjects (Crone et al. 2001) have shown, however, that there are aspects of the cortical response to an auditory stimulus that are not securely phase-locked and therefore would be represented only weakly, or not at all, in the AEP. The properties of these non–phase-locked responses vary across frequency bands and cannot be effectively studied using waveform averaging methods. However, both the phase-locked and non–phase-locked responses can be studied by measuring event-related band power (ERBP), which reflects increases or decreases of total power within given frequency bands with reference to prestimulus background levels (Crone et al. 1998, 2001; Pfurtscheller and Lopes da Silva 1999). In the experiments reported here, we obtained measurements of total ERBP to study both the phase-locked (often termed "evoked"), as well as the non–phase-locked (often termed "induced") components of the auditory event-related responses (see also Pantev 1995). This approach enabled us to explore further the manner in which different human auditory cortical fields process temporal information contained within an auditory stimulus. By using these expanded analytical approaches and stimulus sets, we were able to provide additional evidence supporting our hypothesis of core and belt auditory fields on HG by further characterizing them physiologically, determining more accurately their temporal resolutions and discovering possible additional modes of responsiveness that these auditory cortical fields may use in representing and encoding repeated acoustic transients.

METHODS

Subjects were 15 patients who underwent placement of intracranial electrodes as part of their evaluation and treatment plans for medically intractable epilepsy. Results from experiments on nine of these subjects are described in this study. Experiments on the remaining six were carried out earlier, and although they were more limited in scope and represent preliminary findings, the results are nonetheless fully compatible with those presented here. Research protocols were approved by the University of Iowa Human Subjects Review Board. Informed consent was obtained from each patient enrolled in the study. As part of the treatment plan hybrid depth electrodes (HDEs) were inserted into the HG (Howard et al. 1996b). Subdural grid electrodes were also implanted over the perisylvian cortex, and data obtained from these recordings will be presented in subsequent articles.

Detailed descriptions of the HDEs used in this study and the methods of electrode implantation and subsequent anatomical localization of recording sites have been presented in earlier studies from our laboratory (Brugge et al. 2008b; Howard et al. 1996b, 2000). Briefly, HDEs were guided stereotactically roughly parallel to the long axis of the left HG in four subjects and the right HG in five subjects. Only one HDE was implanted in each subject. Each electrode carried 4 or 6 macro-contacts and 14 micro-contacts that consisted of 40-μm wires with exposed ends cut flush with, or protruding 0.5 mm from, the electrode shaft. Electrodes typically remained in place for ~14 days. Anatomical locations of recording sites were determined using high-resolution CT, structural MRI, and intraoperative photography. When more than one transverse gyrus was present (Figs. 1 and 3), the HDE traversed the most anterior one, which has been shown consistently by cytoarchitectonic criteria to be the location of auditory koniocortex (reviewed by Hackett 2007). One criterion for inclusion in this study was that HDEs be in contact with the HG gray matter along essentially all of their length. There was only one exception to this, which we describe in RESULTS. Wada-test results showed left-hemisphere language dominance for all subjects included in this study. All subjects also had normal hearing based on standard audiometric tests given before implantation surgery. Clinical EEG evaluation indicated that neither the HG nor the immediately adjacent auditory cortical tissue was the site of the epileptogenic foci.

The acoustic stimuli were digitally generated click trains composed of equally spaced rectangular pulses (0.2 ms) delivered through bilaterally placed insert earphones (ER4B, Etymotic Research, Elk Grove Village, IL). The earphones were integrated into custom fitted ear molds of the kind commonly worn by hearing aid users. Click rate was stepped systematically in two experimental series. Series 1 consisted of blocks of six click trains each of ~160-ms duration repeated every 2 s with rates of 25, 50, 100, 125, 150, and 200 Hz. Series 2 consisted of six blocks of click trains each of 1-s duration, repeated every 2 s, with rates of 4, 8, 16, 32, 64, and 128 Hz. For both series, each click-train stimulus was presented 50 times, resulting in a stimulus block consisting of 300 trains. Stimuli within a block were randomly interleaved to reduce the effects of changes in experimental conditions or state of the subject that might have taken place during the 10 min of data acquisition. Recorded electrocorticographic (ECoG) signals were amplified, filtered (1.6–6,000 Hz), and digitized on-line at a sampling rate of 12,207 Hz (TDT RX5 or RZ2 processor, Tucker Davis Technologies). In all cases, the stimulus level was set at a comfortable volume, ~30–50 dB above hearing threshold. Click trains of different rates were held at the same peak amplitude and not energy compensated. Digitized data were stored for later off-line analysis. In our six preliminary studies, click trains of different click rates were delivered in serial order, and data were acquired using either DataWave or Hewlett Packard data acquisition systems.

During recording sessions, the patients were awake and comfortably reclining in a hospital bed or nearby chair situated in a specially designed and constructed electrophysiological recording suite in the University of Iowa General Clinical Research Center (GCRC). This room was quiet and electrically shielded, and a single investigator sat nearby the patient to monitor the session and to be in communication with investigators in an adjoining room that housed the instrumentation for stimulus delivery and data acquisition. In the six preliminary experiments, data were acquired in the epilepsy ward of the hospital.

ECoG data obtained from each recording site on HG were characterized by the AEP and, in the time-frequency domain, by the ERBP. Peak-to-peak measurements were made of the two major deflections occurring in AEPs within a time window of 200 ms after stimulus onset. The ECoG, in response to click train stimulation, may contain both phase-locked (evoked) and non–phase-locked (induced) power. To quantify the phase-locked component, power in the AEP waveform at the stimulus click rate was estimated by multitaper spectral analysis (Mitra and Pesaran 1999; Thomson 1982) using an algorithm implemented in MATLAB (version 7.6.0). The multitaper method is a nonparametric approach to spectral power estimation that has been applied successfully by others to time-frequency analysis of neuronal

electrophysiological data (Compte et al. 2008; Pesaran et al. 2002). The analysis was carried out within the response time window of 0–300 (series 1) or 0–1,000 ms (series 2). Because power at the click rates studied is expected to be found in the ongoing ECoG in the absence of stimulation, reference (baseline) power measurements were made within the period of 300 ms immediately before stimulus onset and compared with power measurements made within the response time window.

The spectral data thus obtained were treated statistically to test whether a click-train stimulus produced a significant change in power from that present in the reference baseline signal. A logarithmic (base-10) transformation of spectral power was obtained and used to define a change-value (response power minus baseline power) for the tested click rates at each of 17 representative recording sites in the nine subjects (in 1 subject, only 1 site was identified, as described in RESULTS). Statistical comparisons were made between the two groups representing posteromedial and anterolateral sites on the HG. The site choices were based on AEP maps obtained for each of the nine subjects (see Figs. 2 and 3). One brain-site group represented a small region on the posteromedial HG that was anatomically consistent with the location of core cortex and that exhibited a robust AEP and FFR characteristic of that area. The second brain-site group was on the anterolateral HG within an area exhibiting low-amplitude, long-latency AEPs and showing no evidence of an FFR. Following Crone et al. (2001), a mixed-effects regression model (Procedure MIXED, SAS v9) was used with change-value as the dependent variable with two fixed-effects predictor variables: brain site with two levels (posteromedial HG and anterolateral HG) and click rate with six (series 1) or four (series 2) levels. Subject was treated as a random effect.

Time-frequency analysis was performed on a trial-by-trial basis using a wavelet transform based on complex Morlet wavelets. ERBP was calculated from power measured in the response window relative to baseline power measured in the 300-ms reference period before stimulus onset. The results of these single-trial calculations were averaged and represented as a plot of power on the time-versus-frequency axis. Details of this analysis can be found in previously published paper from our laboratory (Oya et al. 2002). To distinguish in the time-frequency plane between activity that was phase-locked to the stimulus waveform, the so-called evoked activity, and the event-related but non–phase-locked activity, referred to as induced activity, we followed the approach of Crone et al. (2001) and Steinschneider et al. (2008) by subtracting the AEP waveform from each of the single trial recordings. Although subtraction of the AEP from each trial waveform attenuates phase-locked activity, it does not eliminate it entirely, because the phase-locked response is not perfectly time invariant (see Steinschneider et al. 2008). With this limitation in mind, we were able to compare our estimate of non–phase-locked power with total power.

RESULTS

Despite intersubject variability, a basic pattern of cortical sensitivity to click-train stimulation was observed that was common to all subjects and to both hemispheres. Data obtained from the language-dominant, left hemisphere are first shown in detail for one subject. Figure 1 shows for this subject an MRI of the superior temporal plane showing the trajectory of the HDE with respect to gross anatomical landmarks. The anterior temporal sulcus (*ats*) represents the gross anatomical boundary between the planum polare (PP) and HG, whereas posteriorly, Heschl's sulcus (*hs*) separates the HG from the planum temporale (PT). In this case, as in 4 others in our entire experimental series of 15 subjects, HG appears to be divided along its length by an intermediate sulcus (*is*) into a primary anterior transverse gyrus and a secondary transverse gyrus, labeled on the figure as HG and TG2, respectively (Bailey and Bonin 1951). The distribution of recording sites, which defines the final trajectory of the electrode along the long axis of HG, has been projected onto the cortical surface. The curvi-linear nature of the electrode trajectory is the result of physical distor-

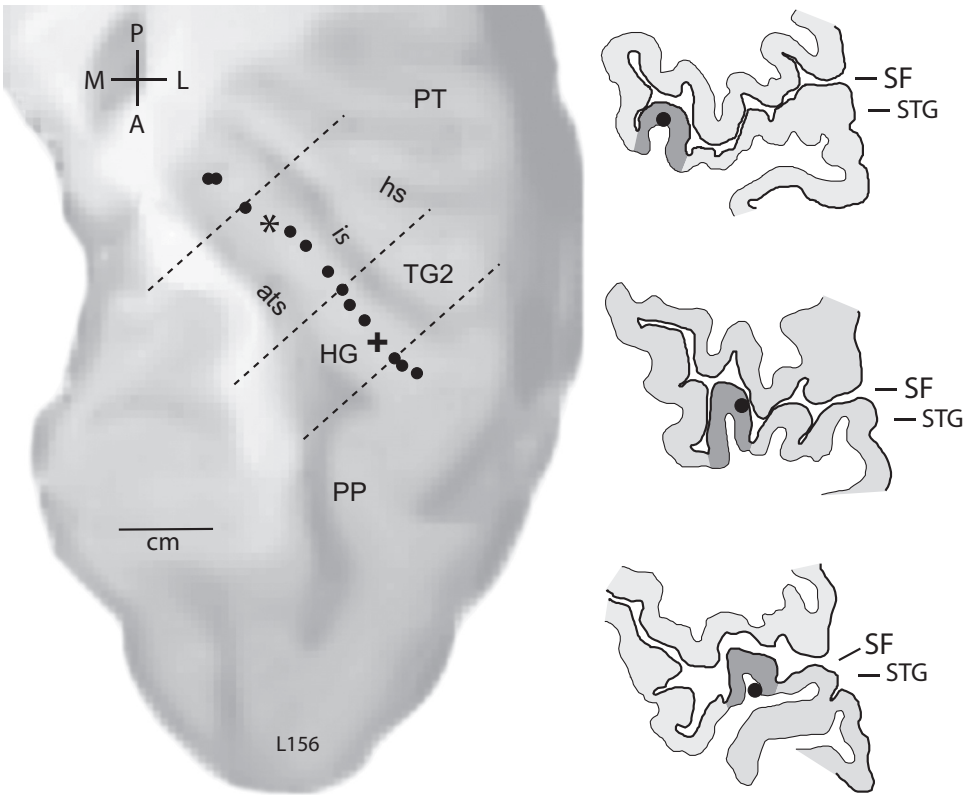

FIG. 1. *Left*: MRI of the superior temporal plane showing the trajectory of the hybrid depth electrode (HDE) with respect to gross anatomical landmarks: PP, planum polare; PT, planum temporale; HG, Heschl's gyrus; TG2, secondary transverse gyrus; *hs,* Heschl's sulcus; *ats,* anterior temporal sulcus. Recording sites, designated by filled circles, are shown projected on the cortical surface. The asterisk and cross mark recording sites, similarly designated on Fig. 2, are within what is interpreted to be the auditory core and belt, respectively. *Right*: cross-sections of the superior temporal plane at the 3 recording locations roughly perpendicular to the long axis of HG (dashed lines on the MRI). Light gray shading represents the cortical gray matter. Darker shading shows the cross-sectional extent of HG. Filled circle within represents the location of the electrode at that recording site.

tion of the superior temporal plane associated with electrode implantation. To the right of the MRI are tracings of three cross-sections taken at the three recording locations roughly perpendicular to the long axis of HG, as indicated by dashed lines on the MRI. Light gray shading represents the cortical gray matter. Darker shading shows what we estimate to be the cross-sectional extent of HG, and the filled circle within represents the location of the electrode at that recording site. In this case, the electrode remained nearly centered on the crown of HG posteromedially, whereas more laterally, it came to lie toward the lateral edge of the gyrus. The electrode remained in contact with the cortical gray matter for most of its length, with the most lateral two or three contacts coming to occupy first the underlying cortical white matter and then gray matter adjacent to HG. Distributions of recording contacts in all nine subjects are shown in Fig. 3.

Series 1: Short click trains

Figure 2 shows AEPs obtained at each of the 14 recording locations in HG shown in Fig. 1 at the indicated click rates,

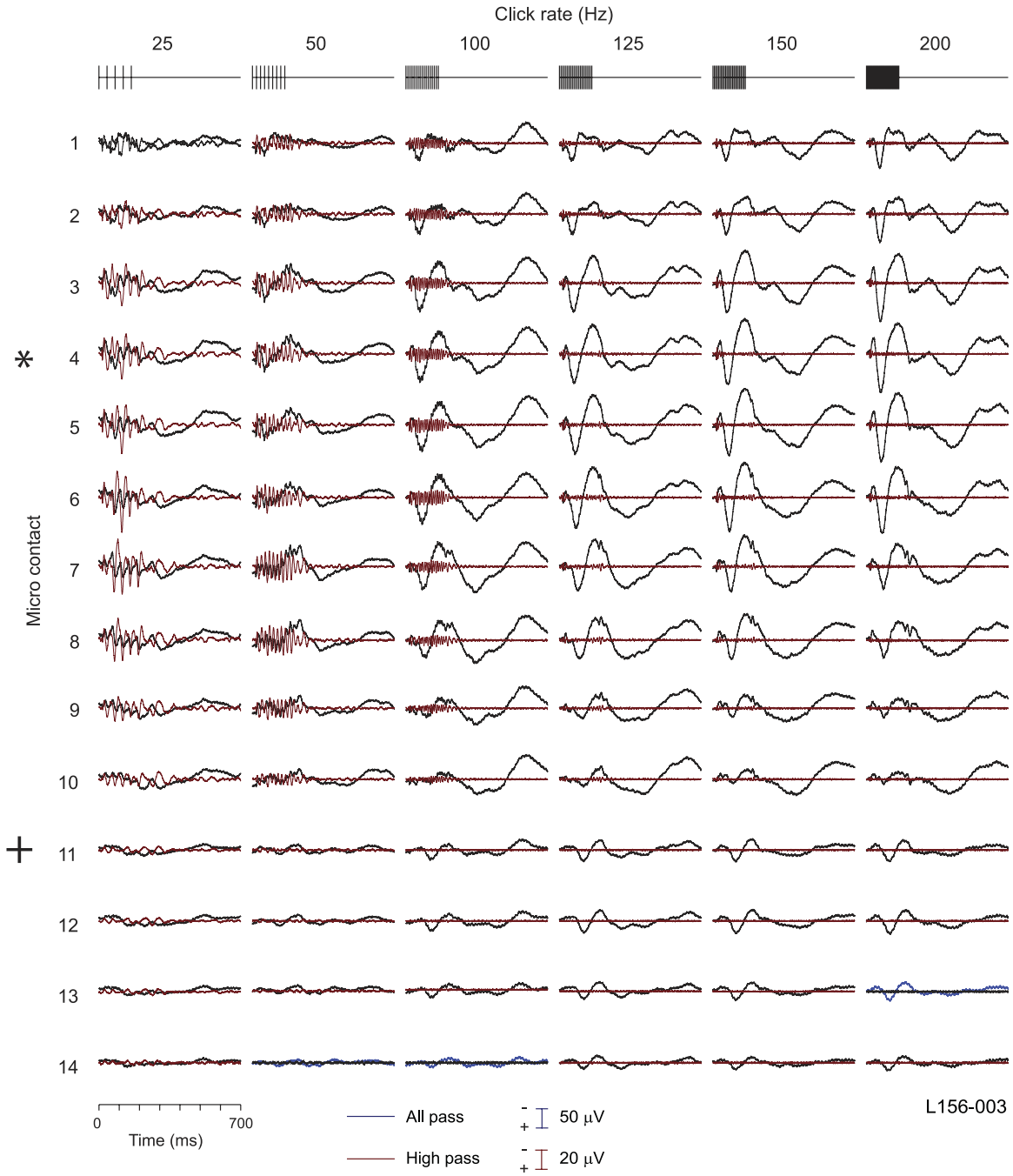

FIG. 2. Series 1: average evoked potentials (AEPs) in response to click trains at 6 click rates at each of the recording sites shown in Fig. 1. All-pass AEPs (black) obtained with filters set between 1.6 and 1,000 Hz. Superimposed high-pass waveforms (red) AEPs obtained with high-pass filter set to 1 octave below the click-train frequency. Click rate and configuration shown across *top* of figure. Stimulus duration: 160 ms. Note the different voltage scale for all-pass and high-pass waveforms.

ranging from 25 to 200 Hz. For further reference, the recording contacts marked by an asterisk and cross refer to anatomical locations as designated in Fig. 1. At each recording locus and for each click rate, two superimposed waveforms are shown. One, shown in black, is the AEP recorded with wide band-pass (1.6–1,000 Hz) filtering, which we refer to as the "all-pass" waveform. The other, shown in red, is the same local field potential after having been passed through a high-pass filter to attenuate the prominent low-frequency components and thereby show the possible presence of a phase-locked FFR. We refer to this waveform as a "high-pass" waveform. To show spatial localization of the FFR, the high-pass cut-off frequency was set one octave below the click rate of the stimulus. Linear filtering was accomplished through a fourth-order Butterworth filter (24 dB/octave). Additional details of the relationship between the stimulus and the FFR for this data set, including a closer look at the all-pass AEP at the lowest click rate in the series, are shown in Fig. 7. Data from the right hemisphere of another subject is shown in supplementary Fig. S1.[1]

Several general observations can be made from these data, which can be applied to results obtained from all experiments in series 1. At click rates of 25 and 50 Hz, the AEP recorded in posteromedial HG tended to be dominated by the FFR. At click rates above 50 Hz, the all-pass polyphasic waveform recorded in posteromedial HG was typically characterized by an early small positive-negative deflection having an onset latency between ~9 and 12 ms (Brugge et al. 2008b; Liegeois-Chauvel et al. 1991), which we interpret to be the manifestation of the thalamocortical afferent volley arriving at the cortex in response to our click stimuli (Steinschneider et al. 1992). This small deflection was usually followed within the next 200 ms by a complex of negative and positive deflections and later by a broad negativity. This dominant waveform recorded at these higher click rates tended to obscure the now diminished FFR. When the AEP was high-pass filtered, however, an FFR could be clearly seen in the time waveform at click rates as high as 125 Hz. We will subsequently show that phase-locking may be reliably detected to ≥200 Hz. The amplitude of both the all-pass and high-pass waveforms tended to be relatively high at a few adjacent recording sites on the posteromedial HG. The amplitude of the AEP diminished systematically with distance from this region of relatively high AEP amplitude. At any given recording location in posteromedial HG, the amplitude of the all-pass waveform grew, whereas that of the FFR declined systematically with increases in click rate. Thus we can attribute the decline in the magnitude of the FFR to limits imposed by the thalamo-cortical afferents or the underlying cortical circuitry, or both, to synchronize to the individual transient events rather than to any overall decrease in effectiveness of the stimulus.

In several subjects (Fig. 3, *A–C* and *E*), the amplitude of the AEP, including the FFR, showed substantial decline medial to the sites of maximal amplitude, but we found no strong evidence for a transition to another field in this region of posteromedial HG. Anterolaterally, however, such a transition was seen to occur as evidenced by the systematic change in both amplitude and morphology of the AEP waveform. Typically the deflections seen on the anterolateral HG within ~200 ms of stimulus onset were greatly diminished in amplitude compared with the posteromedial HG, and in some cases, but not in all, a prominent broad long latency negative deflection appeared. There was little or no evidence of a FFR at the studied click rates in this anterolateral area.

Figure 3 depicts for the nine subjects the changes in peak-to-peak amplitude of the major deflections of the all-pass AEP recorded within 200 ms of stimulus onset as a function of the medio-lateral recording location along the long axis of the HG. The trajectory of the electrode and relative location of recording contacts in each subject are shown (*left*) projected to the surface of the supratemporal plane. Results are not shown for data obtained at 25 and 50 Hz because the all-pass AEP at these click rates exhibited a prominent FFR that interfered with the peak-to-peak measurements. Four plots (Fig. 3, *A–D*) are from data obtained from left hemispheres and five (Fig. 3, *E–I*) from data obtained from the right hemisphere. For eight subjects, the curves derived at different click rate are similar in that relatively high amplitudes were found at a few adjacent sites in posteromedial HG. AEP amplitude fell systematically beyond this region of maximal responsiveness reaching a minimum anterolaterally (dashed line) where it went through a transition before increasing slightly once again. No such transition was seen medial to the sites of maximal amplitude on posteromedial HG even in those cases where the electrode extended far medially on HG and where the peak-to-peak amplitude declined systematically (Fig. 3, *A–D*). In one subject (Fig. 3*I*), there was not the same systematic change in AEP amplitude. We include it, however, because its phase-locked profile did not differentiate it from the other subjects (Fig. 4*I*). As can be seen from the anatomical reconstruction of the electrode contacts in this subject, recordings were made in an anteromedial expansion of what we interpreted to be HG and some distance from the posteromedial area of HG from which the other data were obtained. Our map was simply not extensive enough to determine whether this represents a variant or extension of core cortex on the posteromedial HG.

The systematic decline in temporal synchrony with increasing click rate is shown in Fig. 4 for two representative recording sites, one in the posteromedial HG and the other in the anterolateral HG, in each of our nine subjects. Phase-locked activity was quantified by estimating the power in the AEP waveform at the stimulus click rate by multitaper spectral analysis (see METHODS). Power estimates used as a baseline reference were also obtained during the 300 ms before stimulus onset. By computing power in the AEP rather than in single trials, we sought to extract the phase-locked component from total power that may have constituted the response. Each panel of Fig. 4 shows absolute power (*top*) and logarithmically transformed power (*bottom*) as a function of click rate during the response period (closed symbols) and baseline reference period (open symbols) for each of the subjects. We include baseline power measurements because the ECoG power spectrum is not uniform across the range of frequencies that includes the studied FFR components of the AEP.

In the posteromedial HG of all subjects, the power was greatest at click rates at or below 50 Hz, standing some two to three orders of magnitude above baseline power. Although power declined by several orders of magnitude at a higher click rate, in all cases, it could be seen well above that of baseline out to 100–150 Hz and in some as far as 200 Hz. The situation was quite different at the anterolateral site. Here, for all

[1] The online version of this article contains supplemental data.

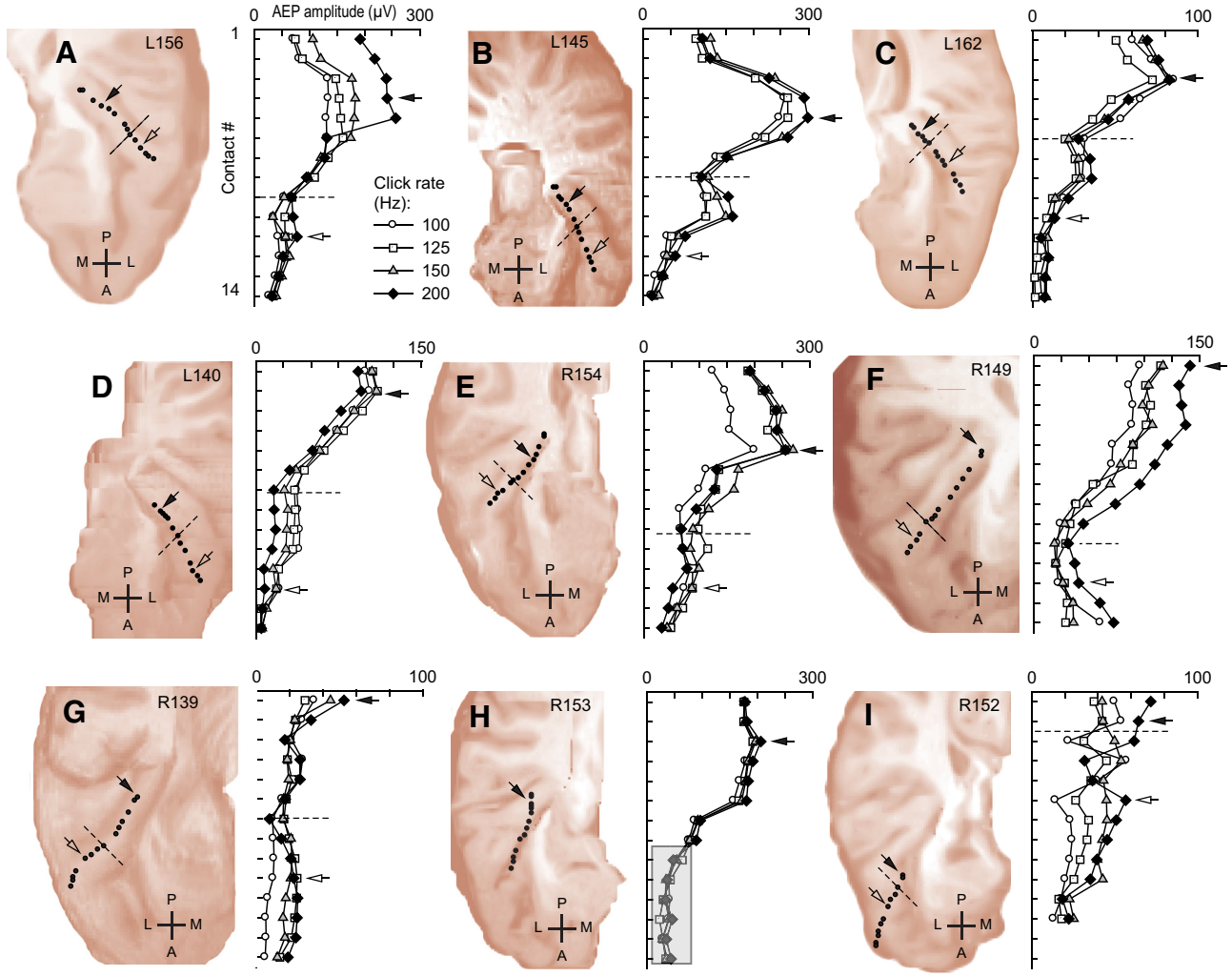

FIG. 3. Series 1: peak-to-peak amplitude of the AEP plotted as a function of contact number for click rates of 100, 125, 150, and 200 Hz for each of 9 subjects. To the *left* of each set of curves is the MRI of the superior temporal plane showing the location of electrode contacts in HG (see Fig. 1 for details). Dashed lines indicate the estimated transition between auditory core and belt fields. Representative contacts within core and belt from which data are presented in Fig. 4 are indicated by closed and open arrows, respectively. The shaded area in *H* identifies those recording sites that fell outside of the gray matter of HG in this subject.

subjects, power remained at or close to baseline at all click rates studied.

The logarithmic transforms of power estimates shown in Fig. 4 were treated statistically, by defining a change-value as log response minus log baseline for the six tested click rates at each of the representative recording sites. A mixed-effect regression model was used to evaluate the fixed effects of brain site (2 levels: posteromedial HG and anterolateral HG) and click rate (6 levels) on change-value (Crone et al. 2001). Subject was treated as a random effect. Figure 5 presents the means and SE for these fixed-effects groups. The main effect for brain site was significant [$F(1,75) = 34.55$, $P < 0.0001$] as it was for click rate [$F(5,75) = 9.16$, $P < 0.0001$], indicating that the power in the AEP relative to baseline recorded in posterolateral HG at the six click rates was significantly greater than that recorded in anterolateral HG. No interaction was found between brain-site and click rate [$F(5,75) = 2.31$]. Follow-up tests were conducted to evaluate all pairwise differences among the change-values within each fixed-effects group ($\alpha = 0.001$, multiplicity correction provided by Scheffe adjustment). There was one significant difference found in the posteromedial group, between 100 and 200 Hz, which is to be expected because there was a systematic decline in phase-locking with increased click rate. There were no significant differences among pairwise comparisons for the anterolateral HG site. Finally, all click rates in the posteromedial HG group produced change-values that were significantly different from zero (*t*-test, $\alpha = 0.0001$). By comparison, there were no change-values in the anterolateral HG population that did so. Thus within this subject population posteromedial HG was distinguished from anterolateral HG based on the former's significant phase-locking, and within this posteromedial HG grouping significant phase-locking to brief click trains was seen to extend to rates at least as high as 200 Hz.

The AEP emphasizes activity that is phase-locked to a stimulus. To study possible non–phase-locked activity in the responses, we computed the ERBP from time-frequency analyses of the same data sets (see METHODS). Figure 6 shows spectro-temporal representations of the ECoG data presented as AEPs in Fig. 2. Several outstanding features were common to all the single-trial data in this series. First, at those posteromedial HG sites exhibiting robust AEPs, an increase in ERBP

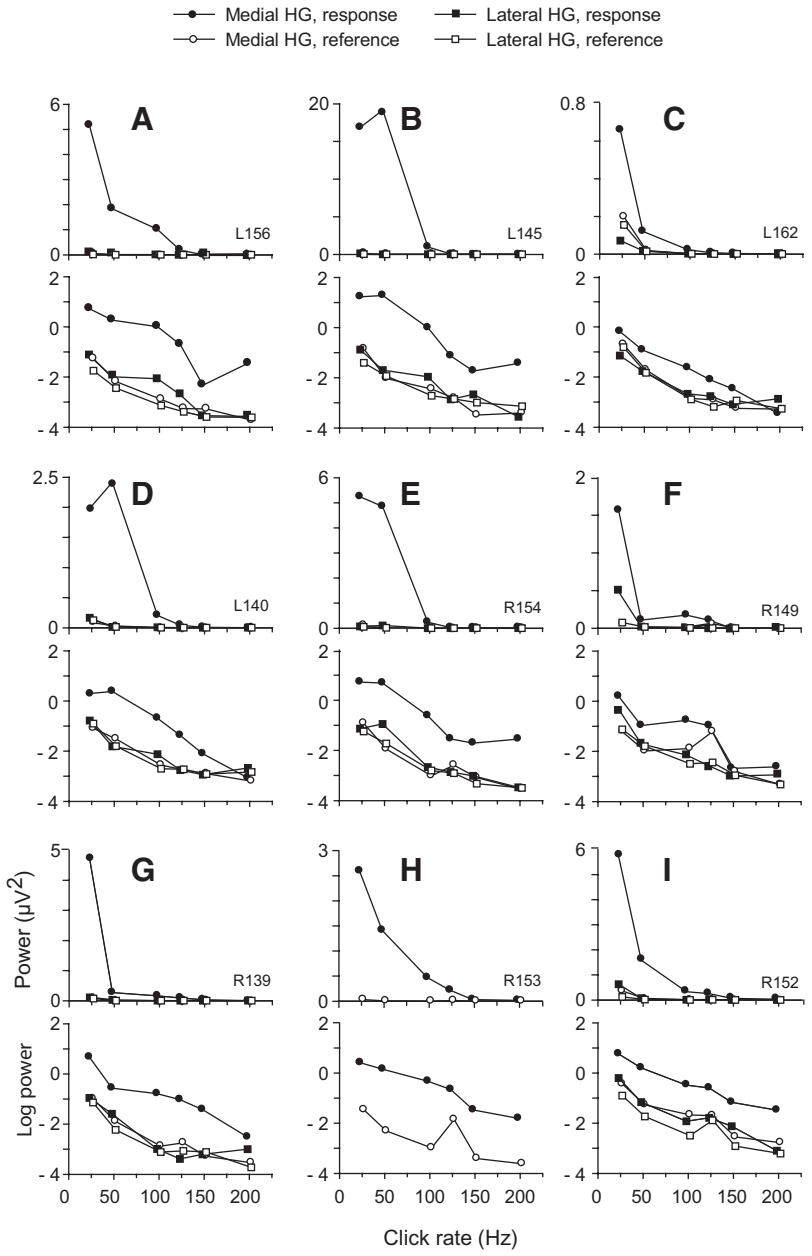

FIG. 4. Series 1: phase-locking to click trains represented as power (*top*) and log power (*bottom*) in the AEP as a function of click rate for the representative brain sites (arrows in Fig. 3) in posteromedial (circles) and anterolateral HG (squares) in 9 subjects presented in Fig. 3. Power measurements made in response (300 ms poststimulus onset) and reference (300 ms prestimulus) intervals of the AEP waveforms are shown by filled and open symbols, respectively.

at gamma frequencies between 70 and 250 Hz was observed throughout the duration of the stimulus. Second, the FFR was represented in these plots as bands of increased power around the frequency of the click train and as bursts of power in the gamma frequency range. These bursts were synchronized to the clicks in the train and thus temporally related to the FFR so prominently represented in the AEP (see also Supplementary Fig. S2).

Details of the relationships between the stimulus and response at the site of maximal responsiveness in posteromedial HG are shown in Fig. 7. As shown in Fig. 7*A*, the FFR was clearly present in the all-pass AEP at click rates as high as 100 Hz and, as shown in Fig. 2, in the high-pass waveform at least as high as 125 Hz. At a click rate of 25 Hz, strong ERBP was evident as dark horizontal bands at 25 Hz and at its two upper harmonics (Fig. 7*A*, horizontal arrows). Harmonics have been recorded as well in auditory-evoked potentials recorded from the scalp (Rees et al. 1986). Time-locked bursts of increased ERBP from ~70 to 250 Hz were also seen (Fig. 7*A*, vertical arrows). Figure 7*B* shows time-frequency plots for the six click frequencies in the series. Phase synchrony in ERBP was evident over the same range of click frequencies that exhibited the FFR (horizontal arrows) with both power at the click frequency and the phase-locked bursts of power in the gamma range.

Patterns of spectral power evoked by the click trains in the anterolateral HG are quite distinct from those in the posteromedial HG (Fig. 6). Gamma activity so prominent in posteromedial sites (1–8) was markedly diminished in anterolateral regions (sites 11–14). A transition zone of intermediate activity was seen around contact sites 9 and 10. Although accurate measurement of the onset time of the ERBP was not possible because of temporal smearing inherent in the wavelet transformation method used, it is clear from the plots shown in Figs. 6

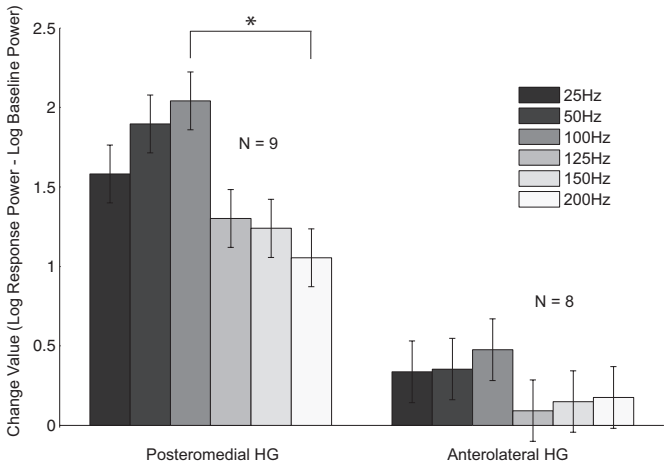

FIG. 5. Means of power change values (±SE) of AEPs recorded from representative posteromedial and anterolateral HG sites shown by arrows in Fig. 3 in response to 6 click rates of series 1. Result of a mixed-effect regression and post hoc analyses given in text.

that the onset latency lengthened markedly in this transition zone between the presumed core and belt fields. Again, as with the FFR, there was no evidence on the anterolateral HG or in the transition zone for temporal synchrony at the click rates studied.

The observation that ERBP mirrored the AEP at lower click rates suggested that much, if not all, of the ERBP was phase-locked power. We will show, however, that there were also prominent non–phase-locked components embedded in the ECoG, and that these had distributions that differed from those of phase-locked components. Before doing so, however, we present data from our experimental series 2.

Series 2: long click trains

The duration of the short click bursts used in series 1 (160 ms) was considerably less than that of the AEP itself, because AEP deflections were seen for as long as 1 s after stimulus onset. The FFR was associated with the major deflections in this 160-ms time period and showed little or no adaptation. These findings extend results of our earlier mapping study using 160-ms duration click trains (Brugge et al. 2008b) and are similar to those previously reported in primary auditory cortex (AI) of the macaque monkey (Steinschneider et al. 1998). However, with 25 Hz being the lowest click rate in this series, we were likely examining rates that extended to the upper limit for robust temporal synchrony. Temporal information in natural sounds extends to even lower frequencies (Rosen 1992). Hence, to examine temporal processing more completely, we carried out a second, complementary, series of experiments using 1-s click trains ranging from 4 to 128 Hz (in octave intervals). This series extended the range of click rates presented in series 1 at the low end while retaining overlapping rates at the high end. In doing so, we also were able to compare our results with data obtained from AI neurons in the marmoset monkey using similar stimuli (Lu et al. 2001) and with AEP results from HG using amplitude modulated noise (Brugge et al. 2008a; Liegeois-Chauvel et al. 2004).

Figure 8 shows all-pass AEPs obtained from the same recording sites from which earlier results of series 1 were presented (see also Supplementary Fig. S3). At the lowest frequencies in the series, it was not possible to use a high-pass filter as we did in series 1. The AEP at all click rates studied were maximal in the posteromedial HG. At low click rates, from 4 to 64 Hz, the FFR was prominent in the AEP, and at each recording site in the posteromedial HG, the amplitude of the early AEP grew while that of the FFR fell with increasing click rate. At a rate of 4 Hz, each click in the train evoked what appears to be a polyphasic waveform reminiscent of those obtained with interclick intervals measured in seconds. This is not surprising, because at 4 Hz, the relatively long 250-ms interclick interval provided sufficient time for the response evoked by one click to subside before the onset of the next. At 8 Hz, the picture changed, and a complex series of deflections, modulated at 8 Hz, was seen. At this click frequency, there was sufficient time (125 ms) for the effects of a one click to impinge on that of the next in the click train and thus the complex waveform became the result of an interaction of overlapping evoked responses. With increasing click rate, the FFR came to resemble cycle-by-cycle entrainment, and by 128 Hz, the all-pass AEP could be characterized mainly by waveforms phase-locked to train onset and offset. The same mixed-effect regression model used in series 1 data was also used to evaluate the fixed effects of brain site (2 levels: posteromedial HG and anterolateral HG) and click rate (4 levels for series 1) on change-value. The outcome of this analysis did not differ from that carried out on Series I.

As seen in Fig. 9, the ERBP tended to mirror the AEP, as we found in series 1 with short-duration click trains (see also Supplementary Fig. S4). The posteromedial HG was characterized by robust phase-locking at low click rates and increasing magnitude at high rates. Phase-locking was preserved throughout the 1 s of stimulation, with adaptation observed with increasing click rate. Anterolaterally, the magnitude of ERBP declined substantially through the transition zone and no phase-locking was in evidence even at the lowest click rate of 4 Hz.

Non–phase-locked power

The time-frequency analysis presented above showed changes in total power associated with click trains of varying rate, which included both the phase-locked and non–phase-locked activity. By subtracting the AEP from each trial at each click rate, we were able to estimate induced activity and compare it to total power in the same time-frequency domain. Figure 10 shows the results of this operation in time-frequency plots for activity recorded in series 1 at click rates of 25 and 125 Hz at sites of maximal amplitude of the AEP in the posteromedial and anterolateral HG. At a click rate of 25 Hz (Fig. 10*A*), frequency following was clearly in evidence in total power (TP), showing up both as a dark horizontal band (arrow) at the stimulus rate and as bursts of phase-locked gamma activity, above ~70 Hz, as described earlier (see Fig. 7). When the all-pass AEP was largely removed from each of the individual trials, thereby yielding an estimate of the non–phase-locked power (NPLP), only the residue of late occurring power around the driving frequency was seen, and the high-frequency FFR was hardly in evidence (Fig. 10*B*). On the anterolateral HG at a click rate of 25 Hz, there was little or no sign of the phase-locked AEP or of ERBP (Fig. 10, *E* and *F*). Thus at a low click rate, the ERBP reflects mainly the time-

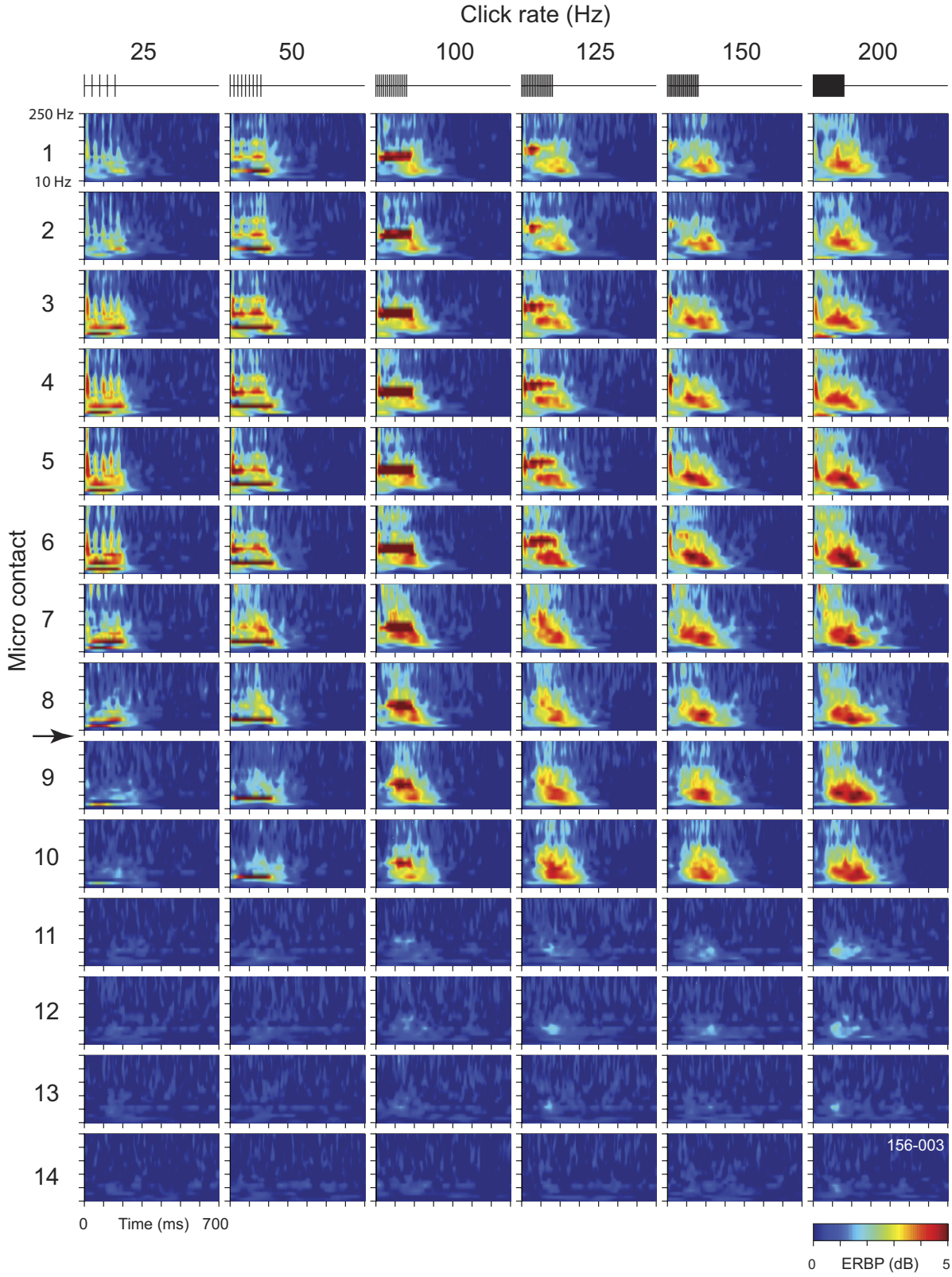

FIG. 6. Time-frequency analysis of data shown in Fig. 2. The analysis, carried out on a trial-by-trial basis, was performed using a wavelet transform based on complex Morlet wavelets. Event-related band power (ERBP) was calculated on a trial-by-trial basis relative to baseline power measured in the 300-ms reference period before stimulus onset (color bar). Results of these single-trial calculations were averaged and represented as a plot of power on the time-vs.-frequency axis.

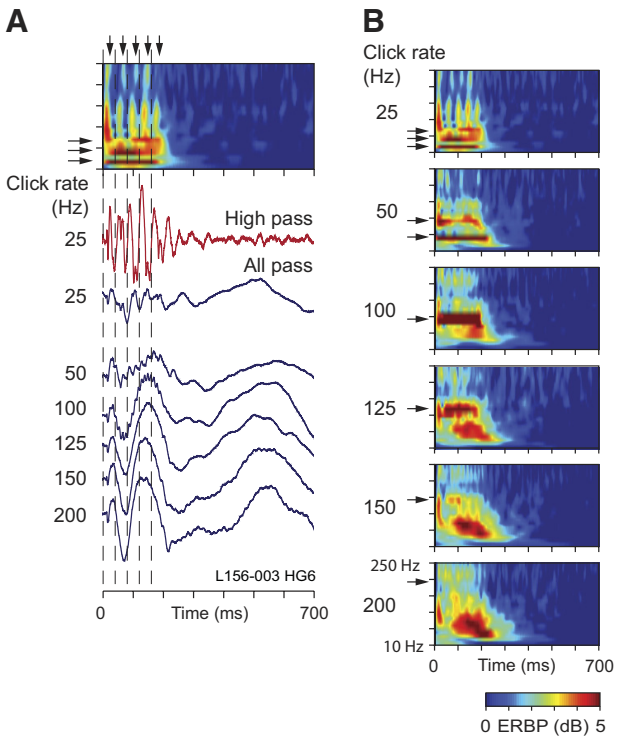

FIG. 7. Temporal relationships between AEP waveform and time-frequency plots for 6 click rates used in series 1. Vertical arrows in *A* indicate peaks of ERBP bursts in response to the 25-Hz click train. Horizontal arrows point to click frequencies and their harmonics.

locked activity observed in the AEP obtained both from posteromedial and anterolateral HG.

At the click rate of 125 Hz, the pattern had changed considerably. Frequency following was again seen reflected in ERBP obtained on posteromedial HG (Fig. 10*C*, arrow). At this click rate, however, robust power increases in the range of 25–100 Hz were also observed, and these increases occurred in a delayed fashion, beginning well after the onset and extending well beyond the offset of the stimulus. When the phase-locked component was removed (Fig. 10*D*), this latter component remained largely unchanged, whereas the FFR was no longer seen. A more striking difference was found in the anterolateral HG. Here, where the AEP was relatively small, there was a robust increase in ERBP, which was dominated by non–phase-locked power.

Extending the findings to longer duration stimuli and to lower click rates (Fig. 11), a similar picture emerged. Here we show the all-pass AEPs superimposed on the time-frequency plot. At a click rate of 4 Hz, the bursts of gamma activity in total power were found associated with the baseline-to-negative phase of the AEP. Removing the AEP from each single-trial response resulted in loss of phase-locked power in the gamma range. Little or no ERBP was seen on the anterolateral HG at this low rate. At 128 Hz, however, there was a brief burst of power at stimulus onset, which was almost entirely time-locked, accompanied by a long-latency non–phase-locked component that extinguished by 200 ms after stimulus onset. Anterolaterally, there was no early onset component, whereas robust, long-latency, non–phase-locked ERBP dominated the response.

The modulation of gamma-band activity seen in presumed core cortex in response to low click rates, is isomorphic with respect to the temporal structure of the stimulus and to the FFR and thus represents the interstimulus interval explicitly (see also Wang et al. 2008). No such explicit representation is seen in the presumed belt cortex on the anterolateral HG. Instead, relatively long-latency non–phase-locked gamma activity arises at higher click rates both in core and belt, reflecting a transformation from an isomorphic to a nonisomorphic representation of the temporal structure of the stimulus. Just how such a transformed signal represents various stimulus attributes is currently under study.

DISCUSSION

Auditory core

Phase-locking to a click-train stimulus, as shown in both the AEP and ERBP, was robust in the posteromedial HG. The magnitude of temporal locking was greatest at click rates below ~50 Hz; it declined sharply above this frequency but could be reliably detected at click rates at least as high as 200 Hz. We interpret this region of HG exhibiting these properties to be the human auditory core cortex. This interpretation is consistent with that arrived at from studies in the awake monkey. Studies in the macaque monkey (Steinschneider et al. 1998) showed that, in the middle cortical layers of AI, the upper limit for temporal synchrony to click trains observed in multiunit activity ranged as high as 150 Hz, whereas synchronous synaptic activity, as shown in current source density measurements, could reach 300 Hz depending on the best frequency at the recording site. The upper boundary for click-train synchrony by single neurons in AI of awake marmoset monkeys was shown to be somewhat lower than this (Lu et al. 2001), although when tested with sinusoidally amplitude-modulated signals, core neurons in New World monkeys were shown to exhibit significant phase-locking at modulation frequencies exceeding 200 Hz (Bieser and Müller-Preuss 1996; Liang et al. 2002). Earlier studies in field AI of the nonanesthetized cat showed phase-locking of the AEP at click rates as high as 200 Hz (Goldstein et al. 1959) and that of single neurons (presumably small stellate cells generating fast spikes) at click rates as high as 1,000 Hz (De Ribaupierre and Goldstein 1972). Because phase-locking is strongest in the thalamocortical input zone of core cortex (Fishman et al. 2000; Steinschneider et al. 1998), differences among studies of temporal synchrony may be attributed to laminae in which recorded neurons were found (see Lu et al. 2001). Furthermore, intracellular studies of auditory cortical neurons have shown the roles played by a balance of excitation and inhibition in influencing temporal precision (Wehr and Zador 2003). Thus the correspondence between human and nonhuman data may even be greater than it first seems if one takes into account the intracortical origins, membrane properties, and firing rates of neurons that may underlie both the AEP and ERBP (Eggermont and Smith 1995; Grenier et al. 2001).

Lu et al. (2001) also reported finding in the marmoset monkey a second, nonsynchronized, population of AI cells that exhibited sustained responses to click trains with firing rates that were monotonic functions of click rate. These findings suggested a dual mechanism for representing repetitive stimuli:

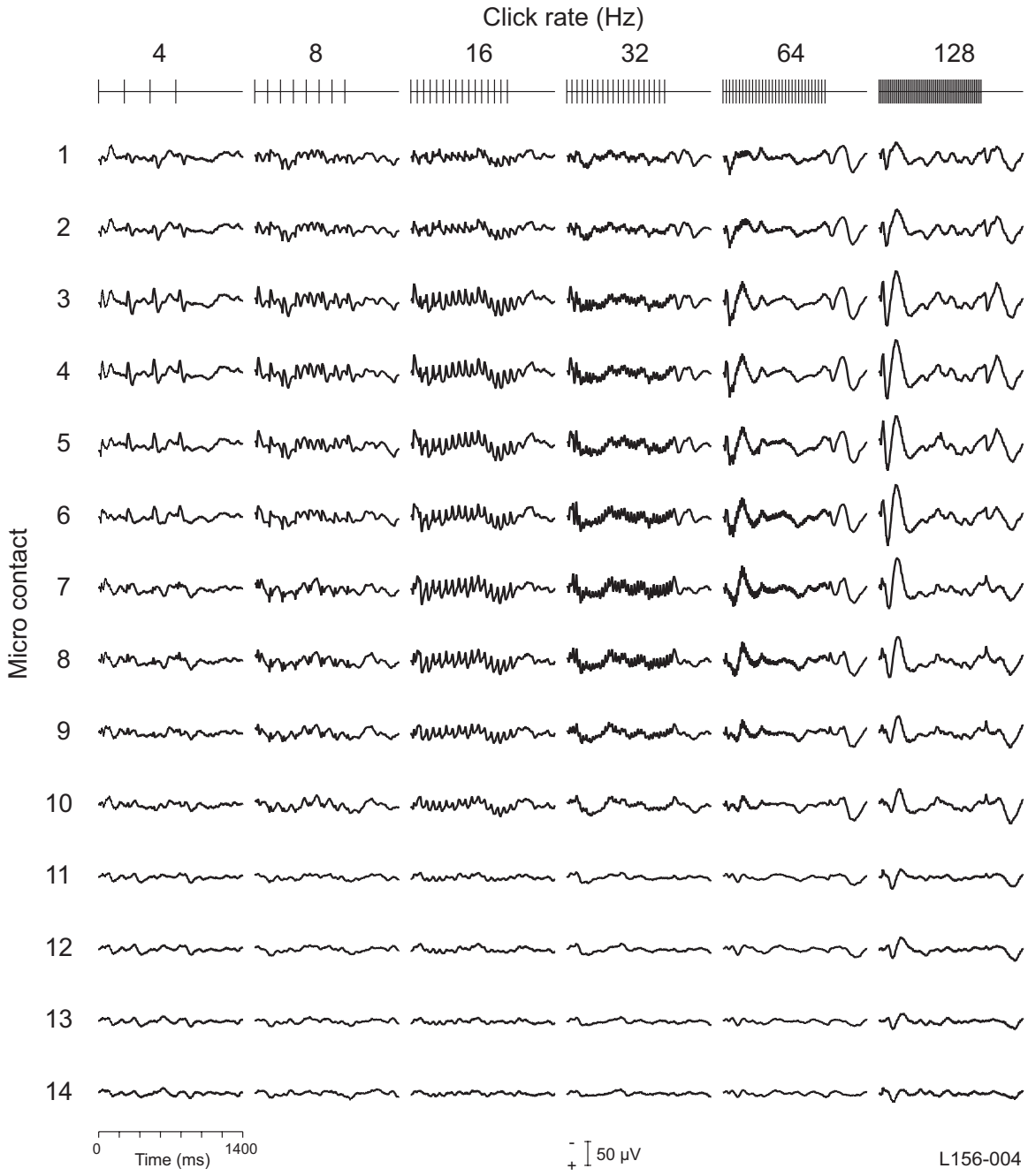

FIG. 8. Series 2: AEPs in response to click trains at 6 click rates at each of the recording sites shown in Fig. 1. Click rate and configuration shown across top of figure. Stimulus duration: 1 s. Filter: 1.6-1,000 Hz.

temporal coding at long interstimulus intervals and rate coding at high intervals (see also Wang et al. 2008). We found that, at higher click rates, where the FFR amplitude declined, there was a concomitant monotonic rise in the peak-to-peak amplitude of the all-pass AEP along a trajectory similar to that found with spike rates of nonsynchronized marmoset AI neurons. Having separated phase-locked from non–phase-locked activity, we also found that, as click rate was increased, the synchronized response became systematically attenuated, mirroring the FFR, whereas the magnitude of the non–phase-locked gamma power became elevated. Our click trains were, however, of the same peak amplitude and duration regardless of click rate. Consequently, changes in click rate were associated with changes in total stimulus energy. Although Lu et al. (2001) reported that phase-locking of AI neurons in marmoset monkeys to compensated and noncompensated click trains was not significantly different, controlling this possible confounding stimulus variable in our experiments will be needed to determine the extent to which changes in the magnitude of the AEP and ERBP were related to click-rate changes per se.

The AEPs recorded using 1-s long click trains (series 2) exhibited phase-locked characteristics, similar to those obtained by Liegeois-Chauvel et al. (2004) using sinusoidal AM noise, indicating that the data from the two studies were likely obtained from the same core field(s) on the HG. These results are also very similar to those derived from EEG (Rees et al.

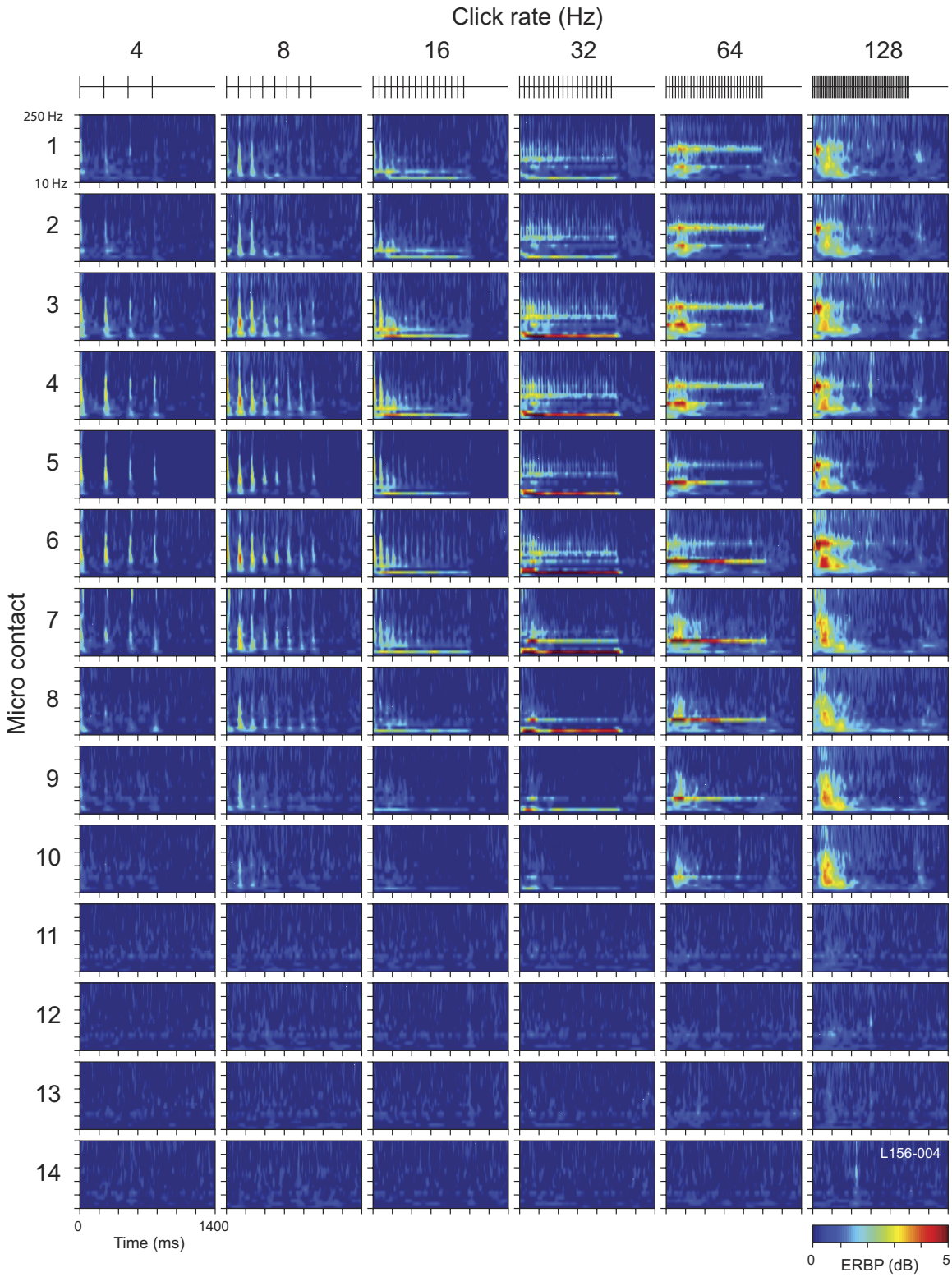

FIG. 9. Time frequency analysis of data shown in Fig. 8. See legend of Fig. 6 for details.

1986) and MEG (Ross et al. 2000) recordings. The band-pass characteristic of temporal modulation functions (MTFs) obtained at very low modulation frequency is often taken as evidence for a filter bank selective for different ranges of modulation frequency (Bieser and Müller-Preuss 1996; Liang et al. 2002; Liegeois-Chauvel et al. 2004). The situation seems more complex than this, however, because the MTF fails to capture the full stimulus-related shape of the AEP waveform. On the basis of responses of AI neurons in the awake macaque monkey to sinusoidal AM stimuli, Malone et al. (2007) have suggested that at modulation frequencies <20 Hz, the processing of modulation signals is better described as an envelope-

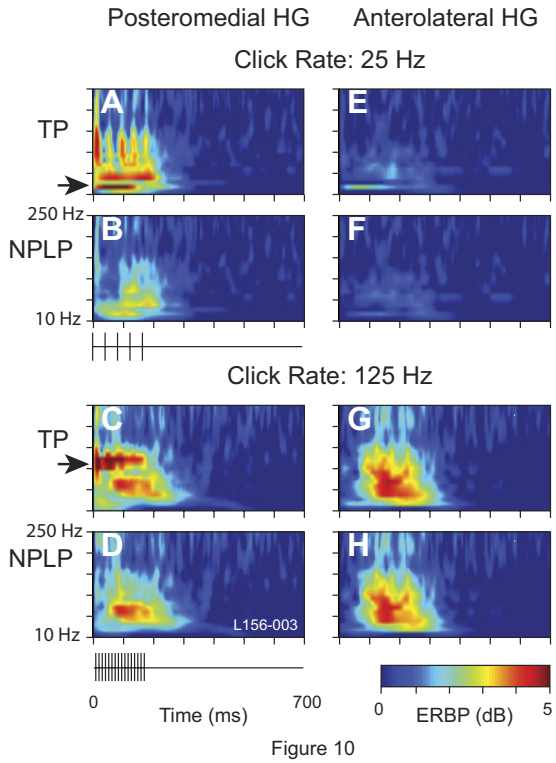

FIG. 10. Time-frequency analysis of data shown in Fig. 2 obtained at recording sites of maximal responsiveness in posteromedial HG (*left*) and anterolateral HG (*right*) at click rates of 25 and 125 Hz. Total power (TP) shown in *top panels* of each pair. Non–phase-locked power (NPLP), obtained by subtracting the AEP from each of the single-trial responses, shown in *bottom panels* of each pair. ERBP color scale and a schematic of the stimulus shown below.

shape discriminator rather than a modulation filter bank. Similarly, in our experiments, the shapes of AEP waveforms, and the stimulus-evoked percepts with which they are correlated, differ markedly across click rates at the lowest frequencies in our series. At a rate of 4 Hz, with an interclick interval of 250 ms, the AEPs to individual clicks in the train were polyphasic and resembled those associated with successive new stimulus events (see Figs 2 and 8 and Supplementary Fig. S3). Liegeois-Chauvel et al. (2004) observed a similar response in AEPs obtained from posteromedial HG to sinusoidally amplitude modulated noise. Because the major deflections in the AEP in response to an acoustic transient are typically completed within this longer interstimulus time interval, they would tend not to exert a strong influence on the response to the next click in the train. Components of the evoked waveform having longer latency and smaller amplitude would, and apparently do, interact to a certain degree even at longer interclick intervals. These interactions were particularly obvious in the AEP when the click rate was raised to 8 Hz, with an interclick interval of 125 ms. Listeners' sensations also change dramatically when the amplitude envelope of a modulated sound is varied over the range of modulation rates used in our study (reviewed by Joris et al. 2004). Amplitude modulations at very low modulation frequency, around a few hertz, are heard as distinct events. This would correspond in our experimental series 2 to a click rate of 4 Hz, where the discrete electrophysiological response seems to mirror the psychophysical percept of individual clicks. The sensation of individual acoustic events gives way at higher modulation rates to one described as "flutter," which in turn undergoes a transition at higher modulation rates to what listeners describe as "roughness." Both of these perceptual categories are paralleled by the temporal synchrony exhibited by neurons of primary auditory cortex of the monkey (Bendor and Wang 2007; Fishman et al. 2000). Eventually the sensation of "pitch" arises, and here again a close relationship is found with a pattern of phase-locked responses of AI neurons of macaque monkey (Steinschneider et al. 1998). The range of click rates over which temporal synchrony is exhibited in core cortex of both human and monkey correlates with human listeners' ability to detect AM of a steady state sound and with perceptual phenomena of acoustic flutter, roughness, and periodicity pitch. The physical attributes associated with these percepts are thus detected and preserved in the auditory core, although the perception itself may be more related to activity arising outside of the core field(s) (Bendor and Wang 2005, 2006; Griffiths 2003; Gutschalk et al. 2004; Hall et al. 2005; Patterson et al. 2002; Penagos et al. 2004).

Cytoarchitectonic studies (reviewed by Hackett 2003, 2007) have shown consistently that auditory core of human is composed of multiple fields, and results of noninvasive functional experiments are consistent with this observation (Formisano et al. 2003; Pantev et al. 1995; Talavage et al. 2004; Yvert et al. 2001, 2005). The multiple-field structure of auditory core cortex of human seems homologous with that of chimpanzees and New World and Old World monkeys (Hackett 2003, 2007). Our experiments using click-train stimulation have not, however, shown, in any given subject, functional boundaries that would signal the presence of more than a single core field. Identifying core fields based on temporal synchrony may have been difficult if, as in monkey, neurons in each of the primary and primary-like fields exhibit phase-locking to amplitude modulated sounds (Bendor and Wang 2008; Bieser and Müller-Preuss 1996). Core fields in monkey have been most clearly identified by their respective tonotopic maps. The tonotopic map obtained in our earlier human experiments showing but a single tonotopic sequence was incomplete, because only a limited range of frequencies and intensities were included in the stimulus set (Howard et al. 1996a). Tone-response data that accompany several of the experiments reported here are based on the AEP, and the frequency and intensity resolutions were simply not sufficiently high enough to place accurately recording locations on a tonotopic map or to show discontinuities or reversals in a tonotopic gradient that commonly signal auditory field boundaries.

There was considerable variation in the gross structure of the HG among our subjects. Because there is no known correlation between gross anatomical landmarks on the HG and underlying cortical structure and function (Hackett et al. 2001; Leonard et al. 1998; Rademacher et al. 1993), we have no independent point of reference by which to relate our functional maps to cortical architecture or to pool data across subjects. There are several other possible sources of functional variability. We may have sampled different primary and primary-like core fields in different subjects. Although neurons in all of core fields of the monkey phase-lock to amplitude modulated sounds, the strength of phase-locking in primary and primary-like fields differs (Bendor and Wang 2008; Bieser and Müller-Preuss 1996). Phase-locking in humans, as in monkeys (Steinschneider et al. 1998), may depend on the cortical laminae and/or the location on the

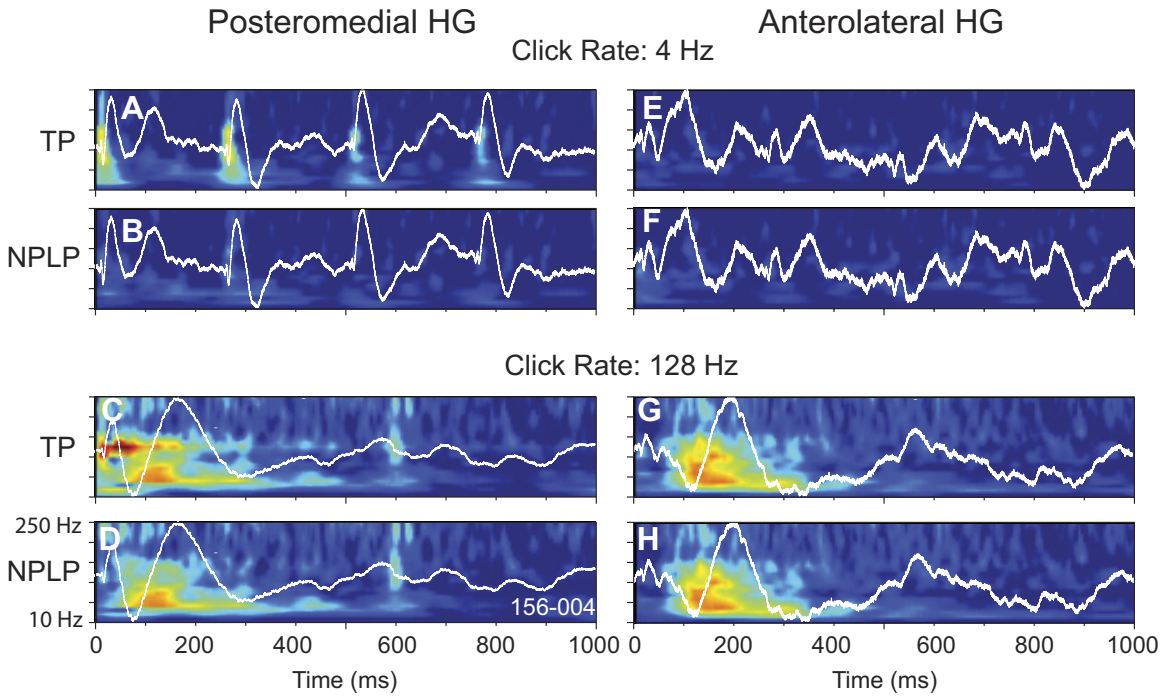

FIG. 11. Time-frequency analysis of data shown in Fig. 8. See legend of Fig. 10 for details.

tonotopic map(s) from which responses were obtained, and we were unable to control for these variables. Finally, plastic changes (Dahmen and King 2007), genetic determinants (Keats et al. 2002), and the history of seizures could well have affected the organization of the central auditory system differently in different subjects. The gross structure of the HG also varies considerably between hemispheres of the same individual (Hackett et al. 2001; Leonard et al. 1998; Penhune et al. 1996; Rademacher et al. 1993). Although Liegeois-Chauvel et al. (2004) reported hemispheric differences in sensitivity to AM sounds, we observed no systematic differences between the two hemispheres with respect to phase-locking to acoustic transients that could be accounted for on the basis of laterality. Our sample sizes are too small, and intersubject variations are too great to draw a firm conclusion on this point.

As Preuss (1995) has pointed out, there are >200 living species of monkeys in the world today, and there is no reason to expect that their brains have all evolved in identical fashions. Nonetheless, taken together, the striking similarity between our electrophysiological results in human core cortex and those obtained from the homologous area in an Old World and a New World nonhuman primate under very similar stimulus conditions suggests that the mechanisms that underlie the encoding of repeated transient acoustic events, and the role these mechanisms play in detecting and perceiving such events at the level of core auditory cortex, may be reasonably conserved across primate species. If so, this may provide an important bridge between auditory cortical processing in humans and nonhuman primates that can be further exploited in future research.

Auditory belt field

Surrounding the human auditory core cortex is a cortical belt composed of possibly seven or eight anatomically distinct areas (Chiry et al. 2003; Rivier and Clarke 1997; Wallace et al. 2002). Homologies with the belt areas identified in the monkey are still largely uncertain (Hackett 2007). In a previous study, we identified electrophysiologically an auditory field on anterolateral HG that we interpreted as being part of an auditory belt system in humans (Brugge et al. 2008b). The AEP recorded there was characterized by relatively low-amplitude, long-latency deflections, in agreement with earlier intraoperative (Celesia 1976) and chronic ECoG studies (Liegeois-Chauvel et al. 1991). In response to click trains of varying click rate, we found that the properties of the AEP recorded there were also clearly distinguishable from those obtained simultaneously from core cortex on the posteromedial HG. The AEP exhibited low-amplitude, long-latency deflections with little or no evidence for a FFR, even at click rates as low as 4 Hz. When examined in the time-frequency domain, phase-locking to clicks was hardly in evidence at any click rate. The non–phase-locked activity, whereas not in evidence at the lowest click rates, was surprisingly robust at high rates, and it occurred with a relatively long latency. Results of functional MRI (fMRI) experiments have identified an area on the anterolateral HG in which sounds having greater pitch salience produced more activity than sounds with no or low pitch salience (Griffiths 2003; Patterson et al. 2002; Penagos et al. 2004). In a related MEG study, Gutschalk et al. (2004) localized evoked activity to the lateral HG that was related to pitch salience and that had a relatively long latency. Bendor and Wang (2005, 2006) have found in monkey auditory cortex "pitch-selective" neurons localized near the anterolateral border of the core field and have suggested that this is consistent with the location of a "pitch-sensitive" area in humans. Unlike the auditory core itself where representation of the physical attributes of the stimulus giving rise to pitch is found, "pitch selective" or "pitch sensitive" regions that span or fall outside the bound-

aries of the core may well be areas where the neural interactions needed for pitch perception per se arise. Liegeois-Chauvel et al. (2004) has reported that "secondary auditory cortex," which may have included anterolateral HG, exhibited phase-locking to sinusoidally amplitude modulated noise, mainly at modulation frequencies of 4 and 8 Hz. Our studies using the same AM sounds showed little or no phase-locked response at these modulation frequencies (Brugge et al. 2008a). Aligning the results of the two studies is difficult because of the different surgical approaches to implantation of the depth electrodes. Thus any apparent differences between the two studies may have resulted from anatomical localization of the recording contacts and interpreting their relationships to the boundary between presumed core and belt areas.

The boundary between the auditory core and this belt field is best characterized as a functional gradient. Such a functional gradient between core and belt fields may correspond to the cytoarchitectonic gradients seen between the auditory core and surrounding auditory fields in both the monkey (Hackett et al. 2001) and cat (Rose 1949). Wallace et al. (2002) identified the cortex of the anterolateral HG as being histochemically distinct from the posteromedial core cortex, naming this area field AL, and suggested that it be considered part of a human auditory cortical belt system. Our anterolateral field, because of its location on the HG with respect to the core, conforms to the histochemically identified field AL. A question arises whether the auditory field on the anterolateral HG should be considered equivalent functionally to one or the other lateral belt field in the monkey (Hackett 2003, 2007). Belt fields in the monkey, which receive their thalamic input mainly from the dorsal division of MGB and cortico-cortical input from each other and from the core, are functionally identified by their neuronal responses to a wide range of acoustic stimuli, including primate and human vocalization. (reviewed by Kaas and Hackett 2005). Thus far we documented differences in temporal response properties between the anterolateral field and the auditory core based on AEP and ERBP analyses. Additional testing using other stimuli similar to those used in monkey experiments is currently being planned or is underway. The results of these experiments will be instrumental in determining the full extent to which the current working model of auditory cortical functional organization (Kaas and Hackett 2005), or some variant of it (see Recanzone 2008), can be applied to humans.

ACKNOWLEDGMENTS

We thank H. Chen, F. Chen, A. Fenoy, and C. Reddy for assistance in data acquisition, C. Kovach for help in data analysis, and C. Dizack for graphic art work.

GRANTS

This work was supported by National Institutes of Health Grants DC-04290 and MO1-RR-59 (General Clinical Research Centers Program), the Hoover Fund, and Carver Trust.

REFERENCES

Bailey P, Bonin G. *The Isocortex of Man.* Urbana, IL: University of Illinois Press, 1951, p. 1–301.

Bendor D, Wang X. The neuronal representation of pitch in primate auditory cortex. *Nature* 436: 1161–1165, 2005.

Bendor D, Wang X. Cortical representations of pitch in monkeys and humans. *Curr Opin Neurobiol* 16: 391–399, 2006.

Bendor D, Wang X. Differential neural coding of acoustic flutter within primate auditory cortex. *Nat Neurosci* 10: 763–771, 2007.

Bendor D, Wang X. Neural response properties of core fields AI, R, and RT in the auditory cortex of marmoset monkeys. *J Neurophysiol* 2008.

Bieser A, Müller-Preuss P. Auditory responsive cortex in the squirrel monkey: neural responses to amplitude-modulated sounds. *Exp Brain Res* 108: 273–284, 1996.

Brosch M, Budinger E, Scheich H. Stimulus-related gamma oscillations in primate auditory cortex. *J Neurophysiol* 87: 2715–2725, 2002.

Brugge JF, Nourski KV, Oya H, Kawasaki H, Reale RA, Howard MA. Representation of sinusoidal amplitude modulated noise within the primary auditory (core) cortex of human. *Soc Neurosci Abstr* 566.6, 2008a.

Brugge JF, Volkov IO, Oya H, Kawasaki H, Reale RA, Fenoy A, Steinschneider M, Howard MA III. Functional localization of auditory cortical fields of human: click-train stimulation. *Hear Res* 238: 12–24, 2008b.

Celesia GG. Organization of auditory cortical areas in man. *Brain* 99: 403–414, 1976.

Chiry O, Tardif E, Magistretti PJ, Clarke S. Patterns of calcium-binding proteins support parallel and hierarchical organization of human auditory areas. *Eur J Neurosci* 17: 397–410, 2003.

Compte A, Reig R, Descalzo VF, Harvey MA, Puccini GD, Sanchez-Vives MV. Spontaneous high-frequency (10–80 Hz) oscillations during up states in the cerebral cortex in vitro. *J Neurosci* 28: 13828–13844, 2008.

Crone NE, Boatman D, Gordon B, Hao L. Induced electrocorticographic gamma activity during auditory perception. *Clin Neurophysiol* 112: 565–582, 2001.

Crone NE, Miglioretti DL, Gordon B, Sieracki JM, Wilson MT, Uematsu S, Lesser RP. Functional mapping of human sensorimotor cortex with electrocorticographic spectral analysis. I. Alpha and beta event- related desynchronization. *Brain* 121: 2271–2299, 1998.

Dahmen JC, King AJ. Learning to hear: plasticity of auditory processing. *Curr Opin Neurobiol* 17: 456–464, 2007.

de la Mothe LA, Blumell S, Kajikawa Y, Hackett TA. Cortical connections of the auditory cortex in marmoset monkeys: core and medial belt regions. *J Comp Neurol* 496: 27–71, 2006.

De Ribaupierre F, Goldstein MH Jr. Cortical coding of repetitive acoustic pulses. *Brain Res* 48: 205–225, 1972.

Eggermont JJ. Representation of a voice onset time continuum in primary auditory cortex of the cat. *J Acoust Soc Am* 98: 911–920, 1995.

Eggermont JJ, Smith GM. Synchrony between single-unit activity and local field potentials in relation to periodicity coding in primary auditory cortex. *J Neurophysiol* 73: 227–245, 1995.

Fishman YI, Reser DH, Arezzo JC, Steinschneider M. Complex tone processing in primary auditory cortex of the awake monkey. I. Neural ensemble correlates of roughness. *J Acoust Soc Am* 108: 235–246, 2000.

Fishman YI, Volkov IO, Noh MD, Garell PC, Bakken H, Arezzo JC, Howard MA, Steinschneider M. Consonance and dissonance of musical chords: neural correlates in auditory cortex of monkeys and humans. *J Neurophysiol* 86: 2761–2788, 2001.

Formisano E, Kim DS, Di Salle F, van de Moortele PF, Ugurbil K, Goebel R. Mirror-symmetric tonotopic maps in human primary auditory cortex. *Neuron* 40: 859–869, 2003.

Fullerton BC, Pandya DN. Architectonic analysis of the auditory-related areas of the superior temporal region in human brain. *J Comp Neurol* 504: 470–498, 2007.

Galaburda AM, Sanides F. Cytoarchitectonic organization of the human auditory cortex. *J Comp Neurol* 190: 597–610, 1980.

Goldstein MH, Kiang NY-S, Brown RM. Responses of the auditory cortex to repetitive acoustic stimuli. *J Acoust Soc Am* 31: 356–364, 1959.

Grenier F, Timofeev I, Steriade M. Focal synchronization of ripples (80–200 Hz) in neocortex and their neuronal correlates. *J Neurophysiol* 86: 1884–1898, 2001.

Griffiths TD. Functional imaging of pitch analysis. *Ann NY Acad Sci* 999: 40–49, 2003.

Gutschalk A, Patterson RD, Scherg M, Uppenkamp S, Rupp A. Temporal dynamics of pitch in human auditory cortex. *Neuroimage* 22: 755–766, 2004.

Hackett TA. The comparative anatomy of the primate auditory cortex. In: *Primate Audition: Ethology and Neurobiology*, edited by Ghazanfar AA. Boca Raton, FL: CRC, 2003, p. 199–219.

Hackett TA. Organization and correspondence of the auditory cortex of humans and nonhuman primates. In: *Evolution of the Nervous System*, edited by Kaas JH. Oxford, UK: Elsevier, 2007, p. 109–119.

Hackett TA, Preuss TM, Kaas JH. Architectonic identification of the core region in auditory cortex of macaques, chimpanzees, and humans. *J Comp Neurol* 441: 197–222, 2001.

Hall DA, Barrett DJ, Akeroyd MA, Summerfield AQ. Cortical representations of temporal structure in sound. *J Neurophysiol* 94: 3181–3191, 2005.

Howard MA, Volkov IO, Abbas PJ, Damasio H, Ollendieck MC, Granner MA. A chronic microelectrode investigation of the tonotopic organization of human auditory cortex. *Brain Res* 724: 260–264, 1996a.

Howard MA, Volkov IO, Granner MA, Damasio HM, Ollendieck MC, Bakken HE. A hybrid clinical-research depth electrode for acute and chronic in vivo microelectrode recording of human brain neurons. *J Neurosurg* 84: 129–132, 1996b.

Howard MA, Volkov IO, Mirsky R, Garell PC, Noh MD, Granner M, Damasio H, Steinschneider M, Reale RA, Hind JE, Brugge JF. Auditory cortex on the posterior superior temporal gyrus of human cerebral cortex. *J Comp Neurol* 416: 76–92, 2000.

Joris PX, Schreiner CE, Rees A. Neural processing of amplitude-modulated sounds. *Physiol Rev* 84: 541–577, 2004.

Kaas JH, Hackett TA. Subdivisions of auditory cortex and levels of processing in primates. *Audiol Neurootol* 3: 73–85, 1998.

Kaas JH, Hackett TA. Subdivisions and connections of auditory cortex in primates: a working model. In: *Auditory Cortex: A Synthesis of Human and Animal Research*, edited by Konig R, Heil P, Budinger E, Scheich H. Mahwah, NJ: Erlbaum, 2005, p. 7–25.

Keats BJB, Popper AN, Fay RR, eds. *Genetics and Auditory Disorders.* New York: Springer, 2002, p. 322.

Leonard CM, Puranik C, Kuldau JM, Lombardino LJ. Normal variation in the frequency and location of human auditory cortex landmarks. Heschl's gyrus: where is it? *Cereb Cortex* 8: 397–406, 1998.

Liang L, Lu T, Wang X. Neural representations of sinusoidally amplitude and frequency modulations in the primary auditory cortex of awake primates. *J Neurophysiol* 87: 2237–2261, 2002.

Liegeois-Chauvel C, de Graaf JB, Laguitton V, Chauvel P. Specialization of left auditory cortex for speech perception in man depends on temporal coding. *Cereb Cortex* 9: 484–496, 1999.

Liegeois-Chauvel C, Lorenzi C, Trebuchon A, Regis J, Chauvel P. Temporal envelope processing in the human left and right auditory cortices. *Cereb Cortex* 14: 731–740, 2004.

Liegeois-Chauvel C, Musolino A, Chauvel P. Localization of the primary auditory area in man. *Brain* 114: 139–151, 1991.

Lu T, Liang L, Wang X. Temporal and rate representations of time-varying signals in the auditory cortex of awake primates. *Nat Neurosci* 4: 1131–1138, 2001.

Malone BJ, Scott BH, Semple MN. Dynamic amplitude coding in the auditory cortex of awake rhesus macaques. *J Neurophysiol* 98: 1451–1474, 2007.

Mitra PP, Pesaran B. Analysis of dynamic brain imaging data. *Biophys J* 76: 691–708, 1999.

Morel A, Garraghty PE, Kaas JH. Tonotopic organization, architectonic fields, and connections of auditory cortex in macaque monkeys. *J Comp Neurol* 335: 437–459, 1993.

Morosan P, Rademacher J, Palomero-Gallagher N, Zilles K. Anatomical organization of the human auditory cortex: cytoarchitecture and transmitter receptors. In: *Auditory Cortex: A Synthesis of Human and Animal Research*, edited by Konig R, Heil P, Budinger E, Scheich H. Mahwah, NJ: Erlbaum, 2005, p. 27–50.

Morosan P, Rademacher J, Schleicher A, Amunts K, Schormann T, Zilles K. Human primary auditory cortex: cytoarchitectonic subdivisions and mapping into a spatial reference system. *Neuroimage* 13: 684–701, 2001.

Oshurkova E, Scheich H, Brosch M. Click train encoding in primary and non-primary auditory cortex of anesthetized macaque monkeys. *Neuroscience* 153: 1289–1299, 2008.

Oya H, Kawasaki H, Howard MA III, Adolphs R. Electrophysiological responses in the human amygdala discriminate emotion categories of complex visual stimuli. *J Neurosci* 22: 9502–9512, 2002.

Pantev C. Evoked and induced gamma-band activity of the human cortex. *Brain Topogr* 7: 321–330, 1995.

Pantev C, Bertrand O, Eulitz C, Verkindt C, Hampson S, Schuierer G, Elbert T. Specific tonotopic organizations of different areas of the human auditory cortex revealed by simultaneous magnetic and electric recordings. *Electroencephalogr Clin Neurophysiol* 94: 26–40, 1995.

Patterson RD, Uppenkamp S, Johnsrude IS, Griffiths TD. The processing of temporal pitch and melody information in auditory cortex. *Neuron* 36: 767–776, 2002.

Penagos H, Melcher JR, Oxenham AJ. A neural representation of pitch salience in nonprimary human auditory cortex revealed with functional magnetic resonance imaging. *J Neurosci* 24: 6810–6815, 2004.

Penhune VB, Zatorre RJ, MacDonald JD, Evans AC. Interhemispheric anatomical differences in human primary auditory cortex: probabilistic mapping and volume measurement from magnetic resonance scans. *Cereb Cortex* 6: 661–672, 1996.

Pesaran B, Pezaris JS, Sahani M, Mitra PP, Andersen RA. Temporal structure in neuronal activity during working memory in macaque parietal cortex. *Nat Neurosci* 5: 805–811, 2002.

Pfurtscheller G, Lopes da Silva FH. Event-related EEG/MEG synchronization and desynchronization: basic principles. *Clin Neurophysiol* 110: 1842–1857, 1999.

Preuss TM. The argument from animals to humans in congnitive neuroscience. In: *The Cognitive Neurosciences*, edited by Gazzanaga MS. Cambridge, MA: MIT Press, 1995, p. 1227–1241.

Rademacher J, Caviness V, Steinmetz H, Galaburda A. Topographical variation of the human primary cortices; implications for neuroimaging, brain mapping and neurobiology. *Cereb Cortex* 3: 313–329, 1993.

Rauschecker JP. Processing of complex sounds in the auditory cortex of cat, monkey, and man. *Acta Otolaryngol Suppl (Stockh)* 532: 34–38, 1997.

Rauschecker JP. Parallel processing in the auditory cortex of primates. *Audiol Neurootol* 3: 86–103, 1998.

Rauschecker JP, Tian B. Processing of band-passed noise in the lateral auditory belt cortex of the rhesus monkey. *J Neurophysiol* 91: 2578–2589, 2004.

Rauschecker JP, Tian B, Hauser M. Processing of complex sounds in the macaque nonprimary auditory cortex. *Science* 268: 111–114, 1995.

Rauschecker JP, Tian B, Pons T, Mishkin M. Serial and parallel processing in rhesus monkey auditory cortex. *J Comp Neurol* 382: 89–103, 1997.

Recanzone GH. Representation of con-specific vocalizations in the core and belt areas of the auditory cortex in the alert macaque monkey. *J Neurosci* 28: 13184–13193, 2008.

Recanzone GH, Guard DC, Phan ML. Frequency and intensity response properties of single neurons in the auditory cortex of the behaving macaque monkey. *J Neurophysiol* 83: 2513–2531, 2000.

Rees A, Green GG, Kay RH. Steady-state evoked responses to sinusoidally amplitude-modulated sounds recorded in man. *Hear Res* 23: 123–133, 1986.

Rivier F, Clarke S. Cytochrome oxidase, acetylcholinesterase, and NADPH-diaphorase staining in human supratemporal and insular cortex: evidence for multiple auditory areas. *Neuroimage* 6: 288–304, 1997.

Rose JE. The cellular structure of the auditory region of the cat. *J Comp Neurol* 91: 409–440, 1949.

Rosen S. Temporal information in speech: acoustic, auditory and linguistic aspects. *Philos Trans R Soc Lond B Biol Sci* 336: 367–373, 1992.

Ross B, Borgmann C, Draganova R, Roberts LE, Pantev C. A high-precision magnetoencephalographic study of human auditory steady-state responses to amplitude-modulated tones. *J Acoust Soc Am* 108: 679–691, 2000.

Steinschneider M, Fishman YI, Arezzo JC. Spectrotemporal analysis of evoked and induced electroencephalographic responses in primary auditory cortex (A1) of the awake monkey. *Cereb Cortex* 18: 610–625, 2008.

Steinschneider M, Reser D, Schroeder CE, Arezzo JC. Tonotopic organization of responses reflecting stop consonant place of articulation in primary auditory cortex (A1) of the monkey. *Brain Res* 674: 147–152, 1995a.

Steinschneider M, Reser DH, Fishman YI, Schroeder CE, Arezzo JC. Click train encoding in primary auditory cortex of the awake monkey: evidence for two mechanisms subserving pitch perception. *J Acoust Soc Am* 104: 2935–2955, 1998.

Steinschneider M, Schroeder CE, Arezzo JC, Vaughan HG Jr. Temporal encoding of phonetic features in auditory cortex. *Ann NY Acad Sci* 682: 415–417, 1993.

Steinschneider M, Schroeder CE, Arezzo JC, Vaughan HG Jr. Speech-evoked activity in primary auditory cortex: effects of voice onset time. *Electroencephalogr Clin Neurophysiol* 92: 30–43, 1994.

Steinschneider M, Schroeder CE, Arezzo JC, Vaughan HG Jr. Physiologic correlates of the voice onset time boundary in primary auditory cortex (A1) of the awake monkey: temporal response patterns. *Brain Lang* 48: 326–340, 1995b.

Steinschneider M, Tenke CE, Schroeder CE, Javitt DC, Simpson GV, Arezzo JC, Vaughn HG. Cellular generators of the cortical auditory evoked potential initial component. *Electroencephalogr Clin Neurophysiol* 84: 196–200, 1992.

Steinschneider M, Volkov IO, Fishman YI, Oya H, Arezzo JC, Howard MA III. Intracortical responses in human and monkey primary auditory cortex support a temporal processing mechanism for encoding of the voice onset time phonetic parameter. *Cereb Cortex* 15: 170–186, 2005.

Sweet RA, Dorph-Petersen KA, Lewis DA. Mapping auditory core, lateral belt, and parabelt cortices in the human superior temporal gyrus. *J Comp Neurol* 491: 270–289, 2005.

Talavage TM, Sereno MI, Melcher JR, Ledden PJ, Rosen BR, Dale AM. Tonotopic organization in human auditory cortex revealed by progressions of frequency sensitivity. *J Neurophysiol* 91: 1282–1296, 2004.

Thomson DJ. Spectrum estimation and harmonic analysis. *Proc IEEE* 70: 1055–1096, 1982.

Tian B, Reser D, Durham A, Kustov A, Rauschecker JP. Functional specialization in rhesus monkey auditory cortex. *Science* 292: 290–293, 2001.

Wallace MN, Johnston PW, Palmer AR. Histochemical identification of cortical areas in the auditory region of the human brain. *Exp Brain Res* 143: 499–508, 2002.

Wang X, Lu T, Bendor D, Bartlett E. Neural coding of temporal information in auditory thalamus and cortex. *Neuroscience* 157: 484–494, 2008.

Wehr M, Zador AM. Balanced inhibition underlies tuning and sharpens spike timing in auditory cortex. *Nature* 426: 442–446, 2003.

Wessinger CM, VanMeter J, Tian B, Van Lare J, Pekar J, Rauschecker JP. Hierarchical organization of the human auditory cortex revealed by functional magnetic resonance imaging. *J Cogn Neurosci* 13: 1–7, 2001.

Woods TM, Lopez SE, Long JH, Rahman JE, Recanzone GH. Effects of stimulus azimuth and intensity on the single-neuron activity in the auditory cortex of the alert macaque monkey. *J Neurophysiol* 96: 3323–3337, 2006.

Yvert B, Crouzeix A, Bertrand O, Seither-Preisler A, Pantev C. Multiple supratemporal sources of magnetic and electric auditory evoked middle latency components in humans. *Cereb Cortex* 11: 411–423, 2001.

Yvert B, Fischer C, Bertrand O, Pernier J. Localization of human supratemporal auditory areas from intracerebral auditory evoked potentials using distributed source models. *Neuroimage* 28: 140–153, 2005.